# We are IntechOpen,
# the world's leading publisher of
# Open Access books
# Built by scientists, for scientists

## 6,900
Open access books available

## 186,000
International authors and editors

## 200M
Downloads

## 154
Countries delivered to

Our authors are among the

## TOP 1%
most cited scientists

## 12.2%
Contributors from top 500 universities

**CLARIVATE ANALYTICS**
**BOOK CITATION INDEX**
**INDEXED**

**WEB OF SCIENCE**™

Selection of our books indexed in the Book Citation Index
in Web of Science™ Core Collection (BKCI)

## Interested in publishing with us?
## Contact book.department@intechopen.com

Numbers displayed above are based on latest data collected.
For more information visit www.intechopen.com

# Ultrafast Nonlinear Optical Response in GaN/AlN Quantum Dots for Optical Switching Applications at 1.55 $\mu$m

S. Valdueza-Felip[1], F. B. Naranjo[1], M. González-Herráez[1],
E. Monroy[2] and J. Solís[3]
[1]*Photonics Engineering Group (GRIFO), Electronics Dept., University of Alcalá,*
[2]*CEA-Grenoble, INAC/SP2M/NPSC,*
[3]*Instituto de Óptica, C.S.I.C.,*
[1,3]*Spain,*
[2]*France*

## 1. Introduction

Multi-terabit optical time division multiplexing (OTDM) networks require semiconductor all-optical switches and wavelength converters operating at room temperature. These devices should be characterized by AN ultrafast response capable of sustaining high repetition rates with low switching energy and high contrast ratio. These features lead to consider the use of resonant nonlinearities for the applications envisaged (Wada, 2004).

There is a particular interest in the development of these devices for the C-band of optical fibers, $\approx$ 1.55 $\mu$m, where erbium-doped fiber amplifiers (EDFAs) are widely available. Highly nonlinear fibers and waveguides have been used for generating nonlinear interactions in this spectral region (Almeida et al., 2004; Bloembergen, 2000). However, due to the low values of their nonlinear coefficients ($n_2 \sim 2.4 \times 10^{-16}$ cm$^2$/W at 1.55 $\mu$m), their implementation often require long interaction distance (even kilometers in the case of nonlinear fibers) or high power levels (González-Herráez, 2011), making them cumbersome for real systems.

An interesting alternative comes through the use of semiconductors. Semiconductor third-order nonlinear optical phenomena, like nonlinear absorption, self- and cross-phase modulation, self- and cross-gain modulation, and four-wave mixing, find direct application in the all-optical control of data streams in fiber-optic networks (Boyd, 2008; Radic & McKinstrie, 2005). An important effort for the development of InGaAs and InGaAsP-based nonlinear optical devices at 1.55 $\mu$m has been performed in recent years (Wada, 2004): FWM wavelength conversion in resonant devices based on InGaAsP-InP waveguides ($\chi^{(3)} \sim 4.2 \times 10^{-10}$ esu) has been reported (Donnelly et al., 1996), as well as all-optical demultiplexing of 160–10 Gbit/s signals with Mach-Zehnder interferometric switch using intraband transitions in InGaAs/AlAs/AlAsSb QWs (Akimoto et al., 2007). However, new materials with larger $\chi^{(3)}$ values are required in order to improve the performance of all-optical-based devices.

From this point of view, III-nitride semiconductors are very good candidates since the asymmetry of their crystalline structure contributes to enhance nonlinear phenomena. There are two different approaches to cover the near-infrared (NIR) spectral range using nitride semiconductors. A first strategy is the use of InN which presents a room temperature direct bandgap $\sim$0.7 eV ($\sim$1.77 $\mu$m). Naranjo *et al.* explored the potential of InN-based structures for slow-light generation by analyzing the third-order susceptibility and the nonlinear absorption at 1.55 $\mu$m (Naranjo et al., 2007; 2011; Valdueza-Felip, 2011).

An alternative approach consists on using intraband transitions in GaN/AlN quantum well (QW) or quantum dot (QD) heterostructures, taking advantage from their large conduction band offset ($\sim$1.8 eV (Tchernycheva et al., 2006)). Using this material system, the resonance frequency can be tuned to 1.55 $\mu$m by controlling the size and composition of the nanostructures. A wide range of intraband devices based on GaN/AlN QWs and QDs have been developed for telecommunication applications in the last decade. In particular intraband QW and QD emitters (Nevou et al., 2008), electro-optical modulators (EOM) (Kheirodin et al., 2008), and different kind of detectors such as: quantum well infrared photodetectors (QWIPs) (Hofstetter et al., 2009), quantum dot infrared photodetectors (QDIPs) (Hofstetter et al., 2010) and quantum cascade detectors (QCD) (Vardi et al., 2008). Furthermore, thanks to the strong electro-phonon interaction, intraband relaxation is faster than interband recombination. As an example, intraband relaxation times in the range of 150–400 fs have been reported in GaN/AlN QWs (Hamazaki et al., 2004; Heber et al., 2002; Iizuka et al., 2006; 2000; Rapaport et al., 2003), confirming the potential of these materials for ultrafast all-optical devices.
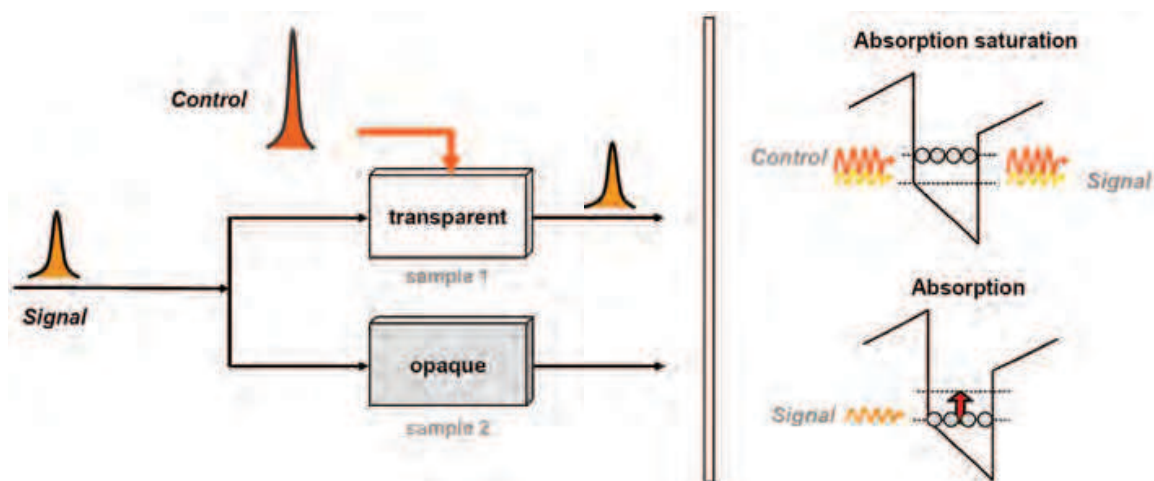


Fig. 1. GaN/AlN-based heterostructure application: ultrafast all-optical switching. The high-intensity pump beam saturates the absorption of the sample making it transparent to the input data beam.

Finally, it is also important to notice that quantum confinement in semiconductor nanostructures enhances the nonlinear response enabling nonlinear interactions at lower power levels, as already demonstrated by second-harmonic generation in GaN/AlN QWs (Nevou et al., 2006). In fact, saturation intensities in the order of 140 MW/cm$^2$ in GaN/AlN QD structures have been reported (Nevou et al., 2009), which correspond to control-pulse switching energies in the order of 10 pJ for optimized waveguide structures (Li et al., 2008; Valdueza-Felip, 2011).

## 2. Samples under study

Due to the rather large electron effective mass of GaN (m* = 0.2m$_0$), layers as thin as 1–1.5 nm are required to achieve intraband absorptions at 1.3–1.55 $\mu$m. Plasma-assisted molecular-beam epitaxy (PAMBE) is the most suitable growth technique for this application, due to the low growth temperature, which hinders GaN-AlN interdiffusion and provides atomically abrupt interfaces (Sarigiannidou et al., 2006). Furthermore, in situ monitoring of the surface morphology by reflection high energy electron diffraction (RHEED) makes possible to control the growth at the atomic layer scale.

The samples described in this work consist of Si-doped GaN/AlN QWs and QDs superlattices (SLs) deposited by plasma-assisted molecular beam epitaxy. The substrates used for the growth of the SLs are 1-$\mu$m-thick AlN-on-sapphire templates grown on the *c*-axis growth direction. Figure 2 shows an schematic description of GaN QWs (a) and QDs (b) analyzed samples. The AlN templates were chosen in order to have crack-free growth (the SL is grown under compressive strain) and a low refractive index in order to optimize the optical guiding in GaN/AlN-based waveguides (Valdueza-Felip, 2011).
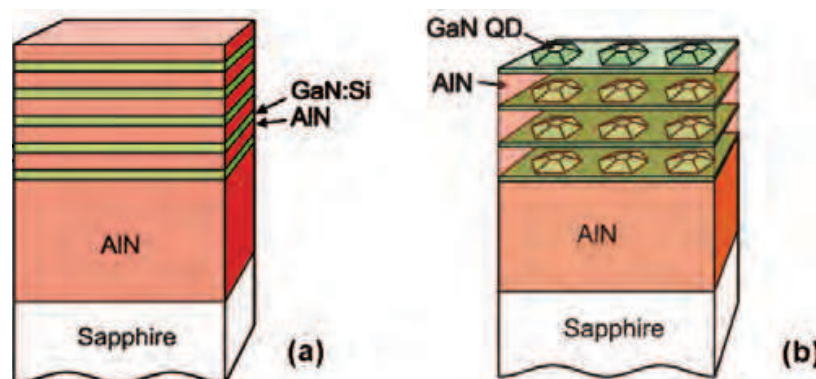


Fig. 2. Structure of the GaN/AlN QW (a) and QD (b) samples under study.

### 2.1 Growth conditions

One fascinating aspect of PAMBE-grown III-V nitride semiconductors is the possibility to control their growth mode by varying parameters such as the substrate temperature or the metal/nitrogen ratio value. As growth mode is directly related with the strain relaxation mechanism of nitride heterostructures, a simple tuning of growth parameters allows growing either two-dimensional (2D) quantum wells (QWs) or three-dimensional (3D) quantum dots (QDs), depending on the desired application.

### 2.1.1 GaN/AlN quantum wells growth

For the growth of GaN quantum wells embedded in AlN barriers, Ga-rich conditions are needed. In particular, GaN optimal growth conditions are under 2 ML of Ga excess for obtaining flat interface surfaces (Adelmann et al., 2003; Kandaswamy et al., 2009; 2008). A substrate temperature above 700°C is required to have a Ga desorption rate high enough to stabilize the Ga bilayer on the growing surface. However, for $T_{sub} \geq 750$°C, the GaN decomposition becomes important. In the case of AlN, the Al flux is fixed to the Al/N stoichiometric value and an additional Ga flux is introduced to stabilize the surface. Since

the Al-N binding energy is much higher than the Ga-N binding energy, Ga segregates on the surface and it is not incorporated into the AlN layer.

The quality of the GaN/AlN heterostructures was found to be particularly sensitive to the Ga/N ratio. The strain fluctuations induced by Si doping and by the presence of the AlN barriers favor the formation of V-shaped pits, even in layers grown in the regime of 2 ML Ga-excess (Hermann et al., 2004; Nakamura et al., 2002). The suppression of these defects has been achieved by an enhancement of the Ga-flux so that growth is performed at the limit of Ga-accumulation. Regarding the growth temperature, it has been observed that overgrowth of GaN quantum wells with AlN at high temperatures results in an irregular thinning of the quantum well thickness due to exchange of Ga-atoms in the GaN layer with Al (Gogneau et al., 2004). This is a thermally activated phenomenon that becomes relevant for AlN growth temperatures above 730°C.

In conclusion, best interface results were achieved at a substrate temperature $T_s$ = 720°C, growing AlN at the Al/N stoichiometry without growth interruptions and using also Ga as a surfactant during the growth of AlN barriers. Under these conditions, the samples present a flat surface morphology with an rms surface roughness of 1.0–1.5 nm measured in an area of $5 \times 5$ $\mu$m$^2$. High-resolution transmission electron microscopy (HRTEM) shows homogeneous QWs, with an interface roughness of ∼1 ML (see interface analysis in ref. (Sarigiannidou et al., 2006)).

### 2.1.2 GaN/AlN quantum dots growth

The synthesis of polar GaN/AlN QDs can be performed by two methods: either by GaN deposition under N-rich conditions (Guillot et al., 2006) or by GaN deposition under Ga-rich conditions followed by a growth interruption (Gogneau et al., 2003). N-rich growth implies a reduction of the mobility of the adsorbed species during growth that results in a high density ($10^{11}$-$10^{12}$ cm$^{-2}$) of small QDs (1–2 nm high). On the contrary, Ga-rich conditions enhance the adatom mobility, leading to a lower QD density ($10^{10}$-$10^{11}$ cm$^{-2}$) and bigger QDs (2–5 nm high). The difference between these growth techniques is illustrated by the atomic force microscopy (AFM) images in Fig. 3, which present QDs resulting from the deposition of 4 MLs of GaN (a) under N-rich conditions and (b) under Ga-rich conditions.
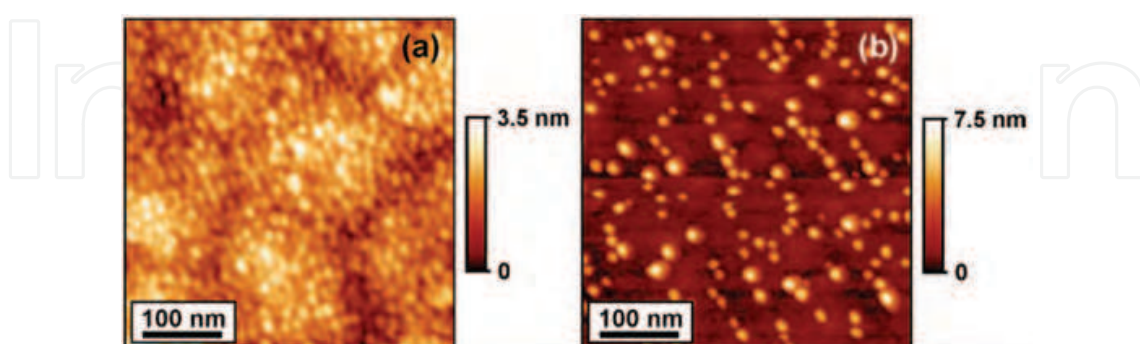


Fig. 3. AFM image of GaN/AlN QDs synthesized by deposition of 4 MLs of GaN under (a) N-rich and (b) Ga-rich conditions. Note that N-rich conditions lead to higher density of smaller QDs whereas Ga-rich conditions lead to lower density of bigger QDs (after Gacevic *et al.* (Gacevic et al., 2011)).

Whatever the growth method, GaN QDs are hexagonal truncated pyramids with $1\bar{1}03$ facets (Chamard et al., 2004), as illustrated in Fig. 4, and no Ga-Al interdiffusion has been observed (Sarigiannidou et al., 2005). They are connected to the underlying AlN by a 2 ML thick defect-free GaN wetting layer.
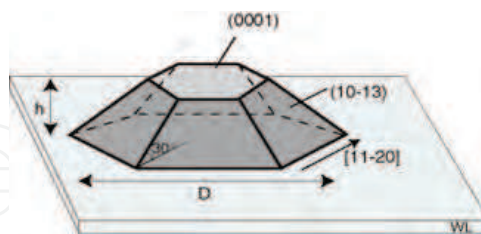


Fig. 4. Schematic representation of a GaN/AlN quantum dot (h = height, D = diamtere, WL = wetting layer).

Si-doping (n-type) is required to populate the first confined electronic level of the nanostructures, enabling efficient intraband absorption. Silicon does not modify the structural quality of the SLs (Guillot et al., 2006). The QDs can be n-type doped by incorporating a silicon flux during the GaN deposition, without modification of the QD growth kinetics or morphology (Guillot et al., 2006).

In order to tune the absorption wavelength within the telecommunication range (1.3–1.55 $\mu$m), the GaN QD height must be reduced down to approximately 1 nm, *i.e.* ∼4 ML. Thus, this QDs must be synthesized using N-rich growth conditions. The QD size can be tuned by modifying the amount of GaN in the QDs, the growth temperature, or the growth interruption time (Ostwald Ripening) (Guillot et al., 2006).

## 2.2 Design of the heterostructures

It is well known that III-nitride materials exhibit spontaneous polarization (Bernardini et al., 1997). Furthermore, depending on the strain state of the layers, an additional (–) or (+) contribution to the total polarization appears, due to the piezoelectric effect. The polarization discontinuity in the well/barrier interface generates an internal electric field that has major consequences for the design of III-nitride intraband devices.

### 2.2.1 Quantum wells design

Kandaswamy *et al.* discussed the specific features of intraband active region design using GaN/AlN materials and showed that the $e_1 - e_2$ intraband transition can be tailored in a wide spectral range from near- to mid-infrared wavelengths by engineering the quantum confinement and the internal electric field by changing the alloy compositions and layer thicknesses (Kandaswamy et al., 2008). In particular, the $e_1 - e_2$ transition energy of GaN/AlN QWs covers the spectral range used for fiber-optic telecommunication networks for a GaN well thickness comprised between 4 and 6 ML (1–1.5 nm). For this work, the GaN/AlN QWs were designed with a well GaN thickness of 5 ML in order to provide a $e_1 - e_2$ intraband transition ∼0.8 eV, which corresponds to ∼1.55 $\mu$m (see Fig. 5).

### 2.2.2 Quantum dots design

Andreev *et al.* have calculated the electronic structure of GaN/AlN QDs using the k×p model and taking the internal electric field into account (Andreev, 2003; Andreev & O'Reilly, 2000;
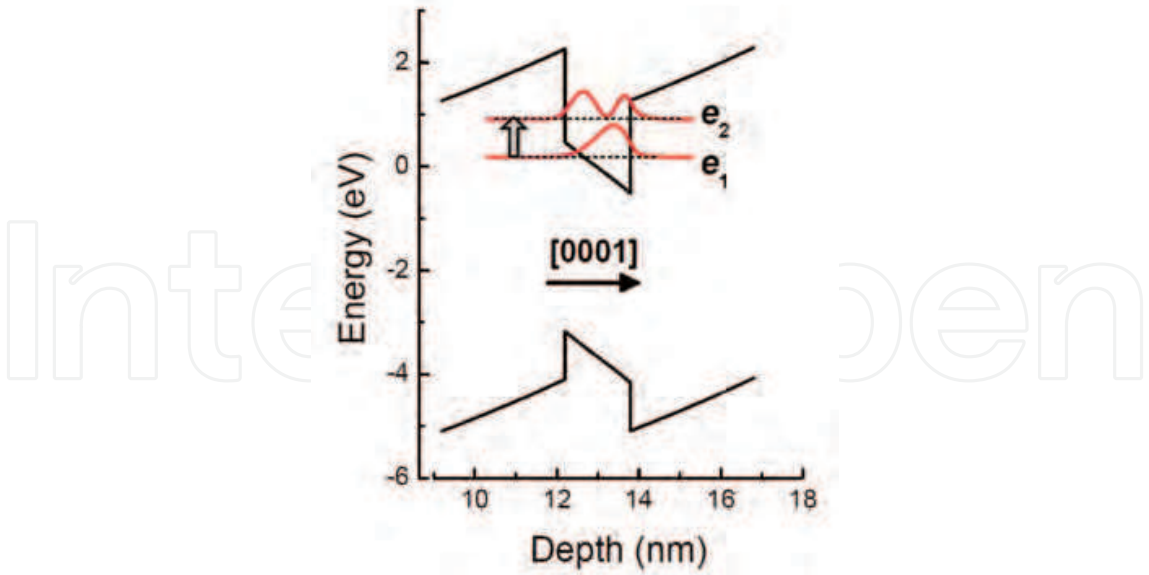
Fig. 5. GaN/AlN QWs band structure. The QWs were designed for having a resonant intraband transition ~1.55 $\mu$m.

2001). These calculations have been complemented by Ranjan *et al.* (Ranjan et al., 2003) using the strong-binding method and a self-consistent treatment to take carrier screening of the electric field into account. From the experimental point of view, infrared absorption peaked at 1.27–2.4 $\mu$m has been observed in GaN/AlN QDs (Guillot et al., 2006; Moumanis et al., 2003; Tchernycheva et al., 2005), associated to the $s - p_z$, intraband transition ($z$ = growth axis), *i.e.* a transition with an optical dipole oriented perpendicular to the (0001) layer plane.
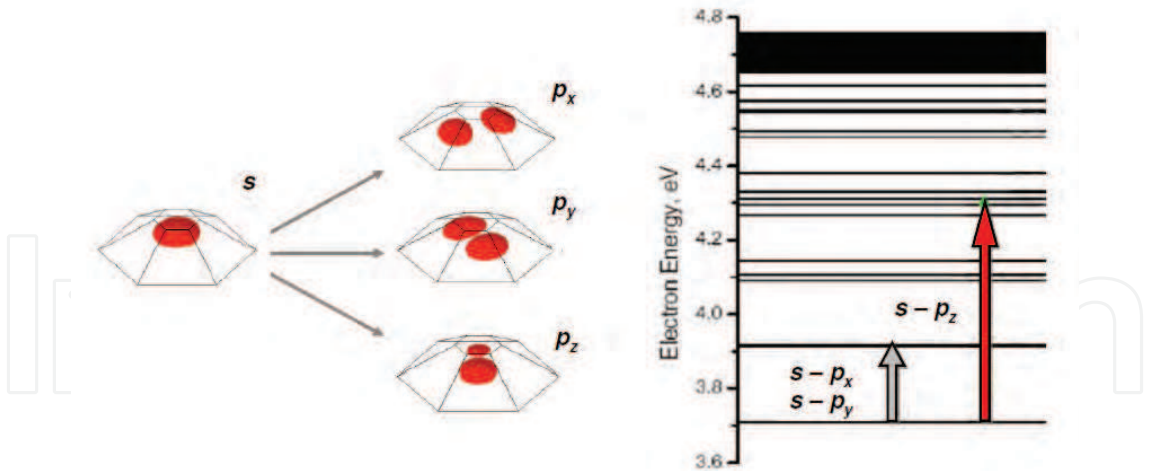


Fig. 6. Electronic states in nitride QDs with transitions $s - p_x$, $s - p_y$ and $s - p_z$ (Andreev, 2003).

Along this chapter, three different samples (S1-S3) are investigated, whose characteristics are summarized in Table 1. Samples S1 and S2 consist of a GaN/AlN QD superlattice containing 20 and 200 QD periods, respectively. The dots present a height of 1.1±0.7 nm and a diameter of 8±2 nm. The samples show a density of QDs in the range of $10^{11}$ cm$^{-2}$, as measured by atomic force microscopy and high-resolution TEM. The GaN QD layers are separated by

3-nm-thick AlN barriers. Sample S3, consists of a 100 period GaN/AlN (1.5 nm / 1.5 nm) QW superlattice. Further details on the growth of the heterostructures can be found in Refs. (Guillot et al., 2006; Sarigiannidou et al., 2006).

| Sample | Structure | Height (nm) | Barrier (nm) | Number of periods |
|--------|-----------|-------------|--------------|-------------------|
| S1 | QD | 1.1 | 3 | 20 |
| S2 | QD | 1.1 | 3 | 200 |
| S3 | QW | 1.5 | 1.5 | 100 |

Table 1. Series of analyzed GaN/AlN heterostructures.

## 3. Structural characterization

The development of devices with a narrow bandwidth depends not only on the in-plane homogeneity of the layers but also on the fluctuations from QW (or QD) to QW (or QD) in the periodic structure. The parameters that might cause vertical inhomogeneities are strain-induced vertical alignment and strain relaxation along the structure by the introduction of misfit dislocations (Guillot et al., 2006).

In order to analyze the strain state of the QD stack, high-resolution x-ray diffraction (HRXRD) measurements were performed. Figure 7 displays the $\theta$-$2\theta$ scan around the (0002) x-ray reflection of a representative QD sample compared to theoretical calculations. The simulation superimposed on the experimental scan was performed assuming that the structure is fully strained on the AlN buffer. It fits the experimental measurement, which indicates that the QD stack is strained on the AlN substrate within the resolution of the measurement (Guillot et al., 2006). Furthermore, the period thickness of the SL is confirmed by measuring the intersatellite (SL0, SL1, SL-1,...) angle in the diffractogram.
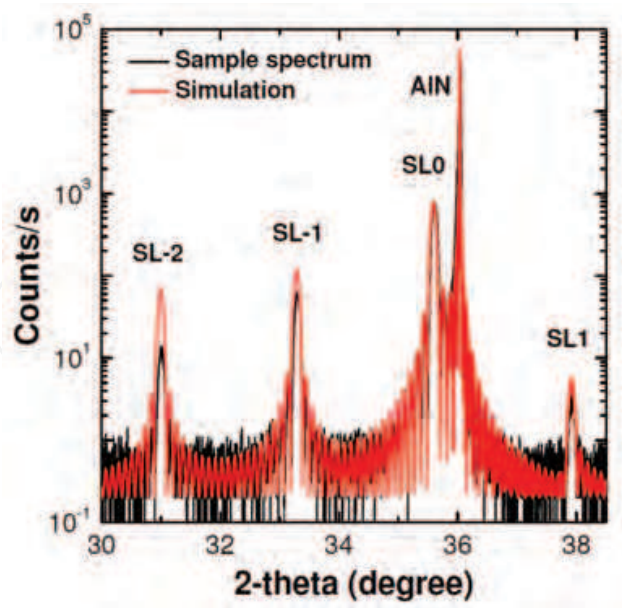


Fig. 7. HRXRD $\theta$-$2\theta$ scan around the (0002) x-ray reflection of a representative QD sample compared to theoretical calculations. SL0, SL1, SL-1, etc. stands for intersatellite diffraction peaks associated with the periodicity of the heterostructure.

The samples were also analyzed by high-resolution transmission electron microscopy (HRTEM) measurements in order to assess the vertical arrangement of the layers. The HRTEM image of the QW sample (S3) of Fig. 8(a) shows abrupt GaN/AlN interfaces, and confirms the narrow quantum wells width ($\sim$1.5 nm) needed for telecommunication applications. No vertical correlation of the QDs is observed. The absence of vertical alignment is explained by the small size and diameter of the QDs (Guillot et al., 2006).

On the other hand, a gradual relaxation of the structure might take place in samples with high density of QDs. Dot coalescence should lead to the generation of misfit dislocations in the GaN wetting layer when its thickness exceeds the critical thickness ($\sim$2 ML) (Guillot et al., 2006). From the HRTEM images, the size of the QDs appears homogeneous along the whole structure, which suggests a negligible relaxation.
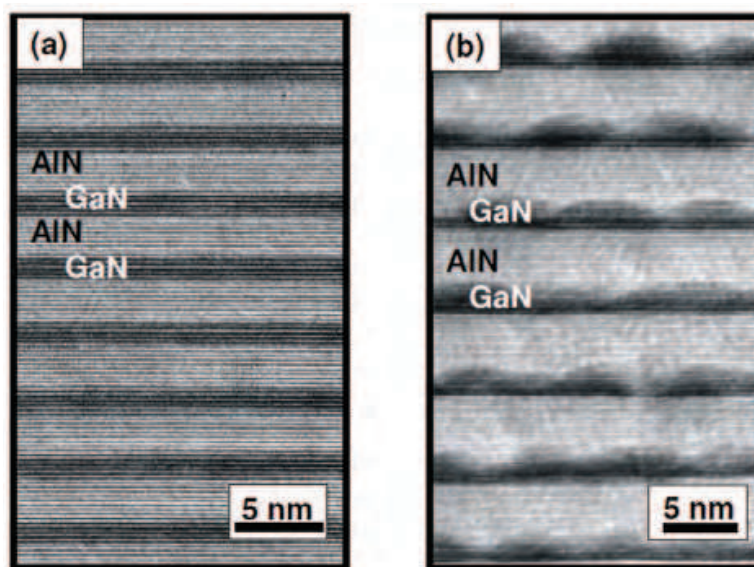


Fig. 8. High-resolution TEM image of a Si-doped GaN/AlN quantum well (a) and quantum dot (b) stack. No vertical alignment of the QDs can be observed.

## 4. Linear optical properties

### 4.1 Photoluminescence

For photoluminescence (PL) experiments the samples were mounted in a cold-finger cryostat with temperature control from $T = 7$ K to RT. PL was excited with a frequency-doubled argon laser ($\lambda$ = 244 nm), and collected into a Jobin-Yvon HR460 monochromator equipped with an ultraviolet-enhanced charge-coupled device (CCD) camera. The diameter of the excitation spot on the sample was about 100 $\mu$m. The excitation power was kept around 100 $\mu$W, low enough to avoid screening of the internal electric field. The low-temperature ($T$ = 7 K) PL spectra of the GaN/AlN QW and QD superlattices with various sizes are presented in Fig. 9(a). By comparison of QW and QD samples, we attribute the broadening of the PL line to the dispersion of the QD size. In the case of the GaN/AlN QWs, the spectral structure of the emission is due to monolayer thickness fluctuations in the QWs, as described elsewhere (Tchernycheva et al., 2006). In the PL from GaN/AlN QDs, the broader line width makes it

possible to observe the superimposition of a Fabry-Perot interference pattern related to the total nitride thickness.

The evolution of the integrated PL intensity as a function of temperature, normalized by the integrated PL intensity at low temperature ($T = 7$ K), is presented in Fig. 9(b) for GaN/AlN QWs and QDs. Keeping in mind that the emission intensity remains stable below 25 K for all the samples, the values presented in Fig. 9(b) should correspond directly to the internal quantum efficiency (IQE) at different temperatures. These results confirm the improved thermal stability of QDs over QWs, as a result of the 3D carrier confinement (Adelmann et al., 2000; Damilano et al., 1999; Gacevic et al., 2011; Guillot et al., 2006; Sénés et al., 2007)

To probe the competition between radiative and nonradiative recombination processes, we now focus on the PL decay time (Renard et al., 2009). Time-resolved PL experiments were performed using a frequency-tripled Ti-Sapphire laser ($\lambda = 270$ nm) with a pulse width around 200 fs. The repetition rate was tuned between 100 KHz and 76 MHz depending on the temporal dynamics studied. The diameter of the excitation spot on the sample was about 50 $\mu$m. The luminescence was collected into a 0.32 m monochromator with a 150 grooves/mm grating, and detected by a streak-camera. The temporal resolution of the setup could reach 5 ps. The samples were mounted in a He-flow cryostat with temperature control from 5 K to room temperature.
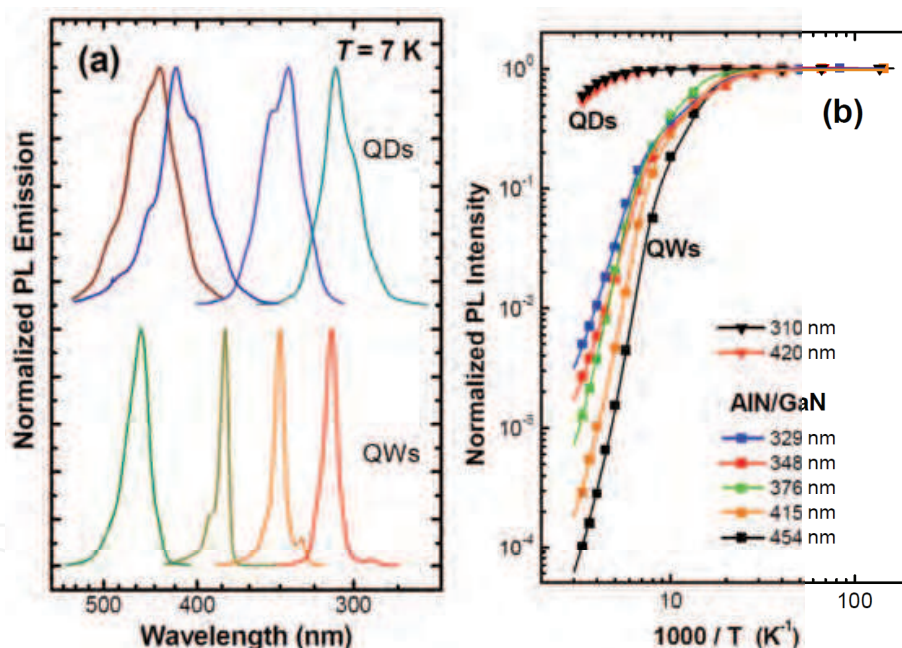


Fig. 9. (a) Normalized photoluminescence spectra of GaN/AlN QD and QW superlattices. The spectra are vertically shifted for clarity. (b) Temperature evolution of the integrated PL emission of GaN/AlN QW and QD samples emitting at different wavelengths. Details about the solid lines fits can be founded in Ref. (Gacevic et al., 2011).

Figure 10(a) displays the PL decay measured in a GaN/AlN QW sample emitting at 415 nm at room temperature and at 5 K. In the inset, the temperature dependence of the $1/e$ decay times measured on the four QW samples emitting at 310, 365, 415 and 455 nm is illustrated. The PL decay times are roughly constant up to 75 K, which strongly suggests that the decay is dominated by radiative recombination at low temperature. However, the decay times

decrease significantly for higher temperatures -typically at least a factor of 2 is already lost at 150 K and at least a factor 10 at room temperature. This is valid for all samples, even for the ones presenting radiative decay times below 1 ns.

In contrast, Fig. 10(b) displays the behavior of a GaN/AlN QD sample emitting at 440 nm, showing thermal insensitivity in all the temperature range. The decay times remain constant as an indication of the inefficiency of nonradiative recombination paths in such structures. The most striking feature is that this is true even for QDs presenting radiative decay times of 500 ns as illustrated in the figure.

Comparing QWs (Fig. 10(a)) and QDs (Fig. 10(b)), nonradiative recombination of photogenerated carriers in the QDs is suppressed in the 4–300 K range. This is a consequence of the 3D confinement in the QDs which, combined with the huge band offset in GaN/AlN, prevents the carrier escape towards nonradiative centers. We can estimate a lower limit for the nonradiative recombination lifetime in the long-lived GaN/AlN QDs of 10 $\mu$s. Conversely, the absence of lateral carrier confinement in QWs favors the thermal diffusion towards nonradiative recombination centers such as dislocations.
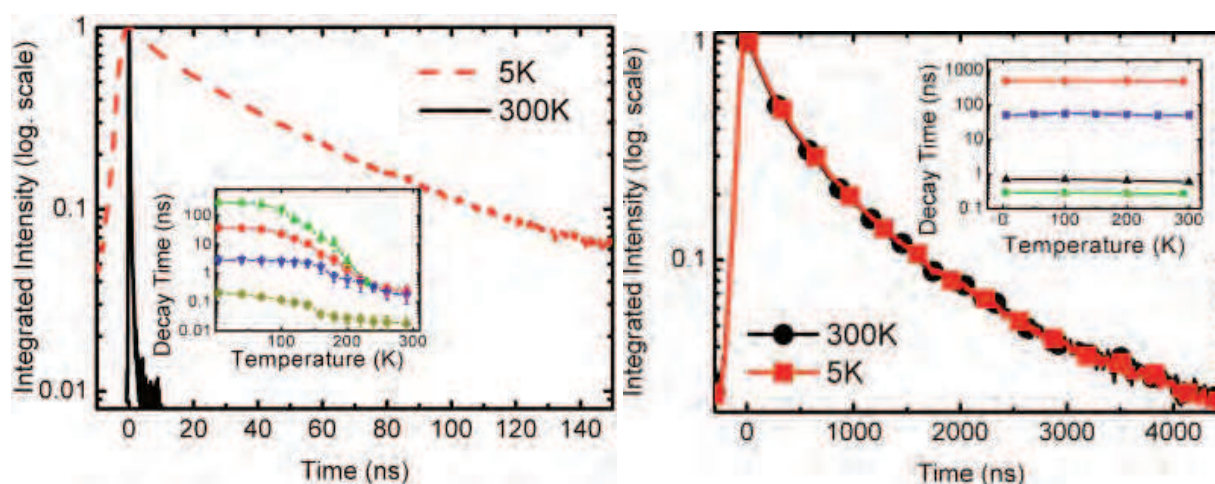


Fig. 10. (a) Comparison of the normalized PL decay at 5 K and room temperature for a sample of GaN/AlN QWs emitting at 415 nm. Inset: Evolution of the decay time of the PL as a function of the temperature for QW samples emitting at 310, 365, 410 and 455 nm. (b) Comparison of the normalized PL decay at 5 K and room temperature for a sample of GaN/AlN QDs emitting at 440 nm. Inset: Evolution of the decay time of the PL as a function of the temperature for QD samples emitting at 310, 340, 400 and 440 nm.

## 4.2 Intraband absorption

In order to assess the NIR absorption, samples were mechanically polished to form a 45° multipass waveguide with 4–5 total internal reflections. The infrared absorption for $p$- and $s$-polarized light was measured at room temperature using a Fourier transform infrared (FTIR) spectrometer. The absorption spectra of samples S1-S3 are illustrated in Fig. 11. For all samples under study, an absorption peak ~1.55 $\mu$m for $p$-polarized light is obtained. No response to $s$-polarized excitation is observed within the measurement spectral range (0.9–4.1 $\mu$m), as expected from the polarization selection rules of the involved intraband transitions ($e_1 - e_2$ in the QWs and $s - p_z$ in the QDs). The broadening of the absorption in the QD

superlattices remains below 150 meV, as a result of QD size fluctuations. On the other hand, the multipeak structure present in the GaN/AlN QW sample can be attributed to ML thickness fluctuations (Tchernycheva et al., 2006).
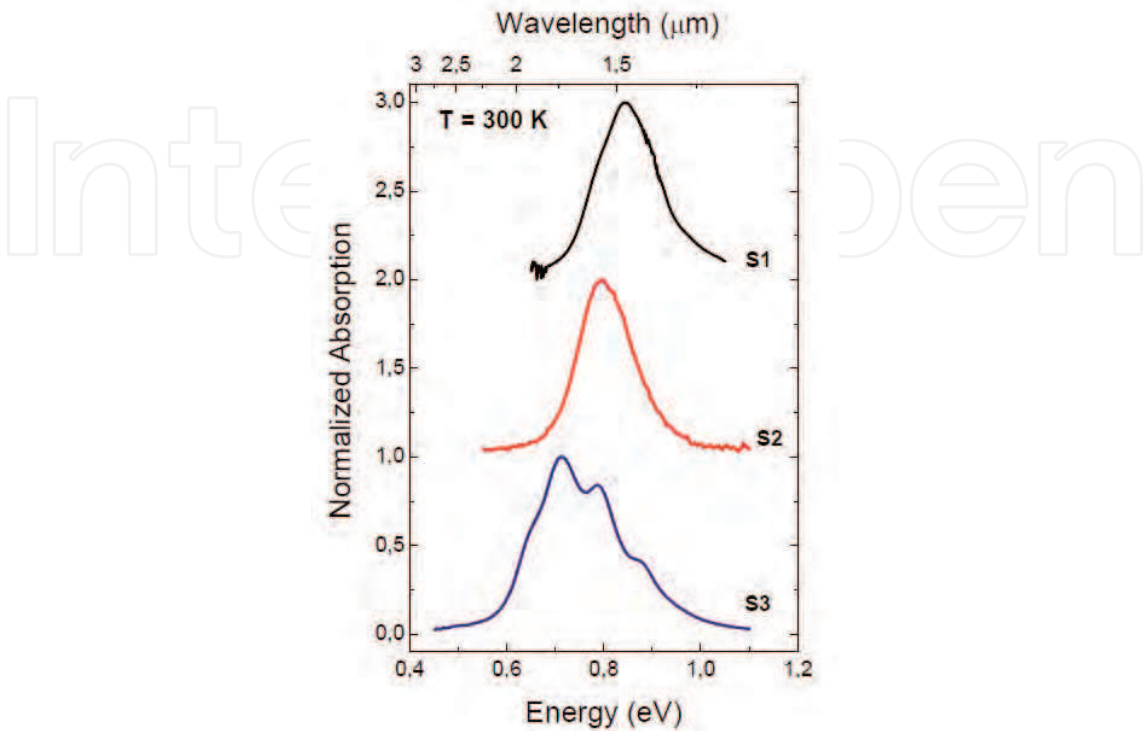


Fig. 11. Normalized infrared absorption from S1-S3 samples under *p*-polarized excitation. The spectra are vertically shifted for clarity. No response to *s*-polarized light was observed for any of the samples in the 0.9 μm < λ < 4.1 μm spectral range.

The spectral dependence of the linear absorption evaluates the linear optical processes associated to the electronic transition. The linear absorption ($\alpha_0$), refractive index, length of the sample ($L_s$), and effective length ($L_{eff}$) are essential parameters to evaluate its nonlinear response. The effective length measures the length over which a lossless material would exhibit the same nonlinear effect as the (lossy) material under study, being calculated by: $L_{eff} = (1 - e^{-\alpha_0 L_s})/\alpha_0$. When $\alpha_0 = 0$, $L_{eff} \cong L_s$ and when $\alpha_0 > 0$, $L_{eff} < L_s$. Thus $L_{eff}$ becomes smaller as the loss increases. Note that as $L_s$ increases, the effective length converges to the value $1/\alpha_0$ (as $L_s \to \infty$, $L_{eff} \to 1/\alpha_0$). In the case of these heterostructures, the length is given by the total length of the active region, *i.e.* the GaN QW (or QD) thickness evaluated along the whole periodic structure. Table 2 summarizes the results obtained from the linear optical characterization at 1.5 μm.

| Sample | Doping (cm$^{-3}$) | Absorption per pass (%) | $\alpha_0 L_s$ | $L_s$ (nm) | $\alpha_0$ (cm$^{-1}$) | $L_{eff}$ (nm) |
|--------|--------------------|--------------------------|----------------|------------|-------------------------|-----------------|
| S1 | $10^{20}$ | 1.6 | 0.032 | 24 | $13.4 \times 10^3$ | 23.6 |
| S2 | $5 \times 10^{19}$ | 10 | 0.23 | 200 | $11.3 \times 10^3$ | 179 |
| S3 | $5 \times 10^{19}$ | 4.2 | 0.088 | 150 | $5.8 \times 10^3$ | 144 |

Table 2. Summary of the results obtained from linear optical measurements at 1.5 μm.

## 5. Nonlinear optical characterization

### 5.1 Third-order nonlinear effect: four-wave mixing

High-intensity lasers enable a variety of interesting nonlinear optical phenomena such as the generation of new frequencies from monochromatic light in a nonlinear medium. At the excitation intensities applied to generate these nonlinear effects, the optical parameters of the pumped material become a function of the light intensity. In nonlinear optics regime additional terms have to be considered in the polarization density to properly explain the behavior of light propagating through a nonlinear medium. For small nonlinearities $\mathbf{P}(t)$ can be expressed as a function of the applied electric field $\mathbf{E}(t)$ by the superposition of both linear and nonlinear polarization components (Boyd, 2008; González-Herráez, 2011) as:

$$\mathbf{P}(t) = \mathbf{P}_L + \mathbf{P}_{NL} \tag{1}$$

where $\mathbf{P}_{NL} = \mathbf{P}^{(2)} + \mathbf{P}^{(3)} + \cdots$ are the nonlinear polarization terms that depend on the applied electric field. The optical control of light in communication networks is performed thought the use of third-order nonlinear optical phenomena like the Kerr-effect-based four-wave mixing (FWM) process.

The optical **Kerr effect** is a change in the refractive index of a material in response to an applied electric field. This induced index change is proportional to the square of the electric field. Considering a material under a single, monochromatic wave oscillating at the fundamental frequency $\omega$, the total polarization can be described by a scalar expression (González-Herráez, 2011; Shutherland, 2003) as:

$$P_\alpha(\omega) = \epsilon_0 \left( \chi^{(1)}(\omega)E_\alpha(\omega) + 3\chi^{(3)}_{\alpha\beta\gamma\delta}(\omega)|E|^2 E_\delta(\omega) \right) \tag{2}$$

where $|E|^2$ is the amplitude of the electric field and $\chi^{(3)}(\omega)$ denotes the third-order susceptibility parameter. In this equation, the nonlinear term $3\chi^{(3)}(\omega)|E|^2$ is treated as a perturbation (small variation) of the linear term, *i.e.* a correction to the linear susceptibility that depends on the input intensity ($|E|^2 \propto I$).

Assuming that the index and absorption changes are an instantaneous function of the applied electric field, the material response can be described by $n(I) = n_0 + n_2 I$ and $\alpha(I) = \alpha_0 + \alpha_2 I$, where the nonlinear refractive index $n_2$ and nonlinear absorption coefficient $\alpha_2$ are related to the third-order nonlinear susceptibility. In weakly absorbing media the real part of $\chi^{(3)}$ drives the nonlinear refraction while the imaginary portion characterizes the nonlinear absorption (Shutherland, 2003) as:

$$n_2 = \frac{3}{4} \frac{1}{n_0^2 \epsilon_0 c} \Re e \left[ \chi^{(3)} \right] \tag{3}$$

$$\alpha_2 = \frac{3\pi}{\lambda} \frac{1}{n_0^2 \epsilon_0 c} \Im m \left[ \chi^{(3)} \right] \tag{4}$$

Since the nonlinear polarization depends on $\omega$, the $\chi^{(3)}$ parameter varies when the material is in resonance with the input beam frequency. Thus, in the case of strongly absorbing media a more complex treatment must be considered following the description reported in Ref. (del Coso & Solís, 2004).

**Four-wave mixing** through optical phase conjugation is a useful experimental technique for the characterization of third-order nonlinear materials (Sheik-Bahae et al., 1990). FWM is an intermodulation phenomenon in optical systems, whereby interactions between 3 waves in a nonlinear medium produces a 4th wave via the third-order polarization (Hill et al., 1978; Inoue, 1992). It is possible, using nonlinear optical processes, to reverse the phase of a beam of light. The reversed beam is called conjugate beam.

Figure 12 shows an abstract drawing of the FWM process, where three coherent waves are incident on a nonlinear medium, and a fourth wave (the phase-conjugated one) is generated. In a simplified gratings formalism (not valid for beams with crossed polarizations), the generation of the conjugated signal (beam) can be viewed as follows. The conjugated beam is produced by the refractive index modulation caused by the interference of two of the beams forming a phase grating. Two of the beams ($\mathbf{E}_1$ and $\mathbf{E}_2$ or pump beams $p_1$ and $p_2$) interfere and "write" a real-time diffraction pattern or phase grating, while the third beam ($\mathbf{E}_3$) "reads" (or probe, $s$ beam) the grating. The diffraction of the third beam when propagating through the grating generates the fourth beam ($\mathbf{E}_4 = \mathbf{E}_c^*$, the $c$ beam), whose phase is conjugated to the three incident beams (Zeldovich et al., 1985). The diffracted phase-conjugated beam is transmitted by the material in a direction determined by the wave vectors of the interacting photons. In the degenerate case ($\omega_1=\omega_2=\omega_3=\omega_4=\omega$) energy and momentum conservations implies that that the sum of the wave vectors of $\mathbf{E}_1$ and $\mathbf{E}_2$ should be equal to the sum of the wave vectors of $\mathbf{E}_3$ and $\mathbf{E}_4$. In this work, the third-order nonlinear susceptibility $\chi^{(3)}$
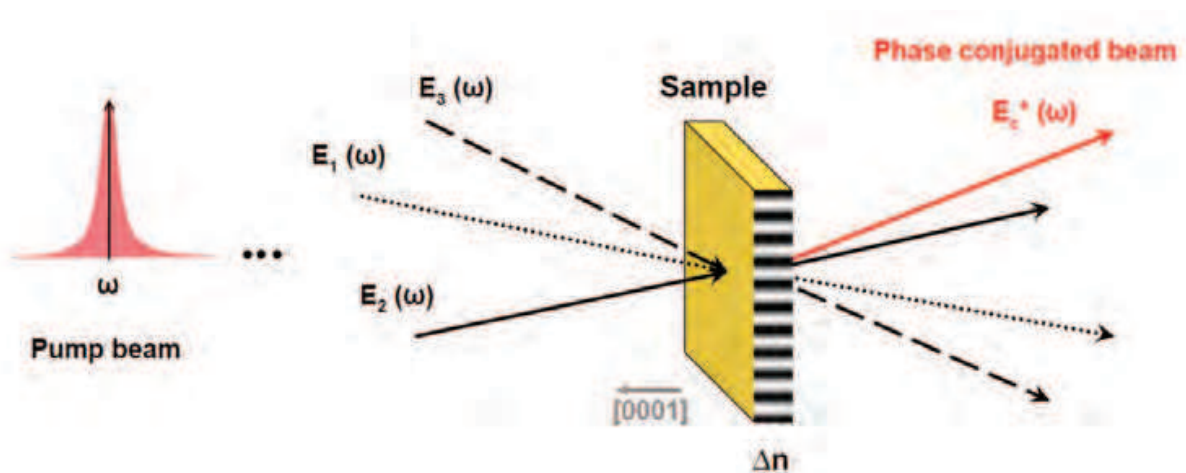


Fig. 12. Schematic of phase conjugation via the perturbation of the refractive index through the third-order nonlinear susceptibility.

of III-nitrides is studied by resonant degenerate four-wave mixing (DFWM) in the forward boxcars configuration. In this configuration, three parallel and co-propagating input pulsed laser beams are focused simultaneously in space and time on the sample with a lens. The $z$ direction is the direction of propagation of the beams before the lens, normal to the surface of the sample. If the three input beams are placed in the three vertices of an square centered at the lens, the energy and momentum conservations ($\sum \mathbf{k_i}=0$) is guaranteed and enables the generation of the conjugated fourth beam at the output of the sample (Shutherland, 2003).

Figure 13 illustrates the experimental setup used for DFWM measurements. The excitation source is an optical parametric amplifier (OPA)´which operates at 1 kHz and provides 100
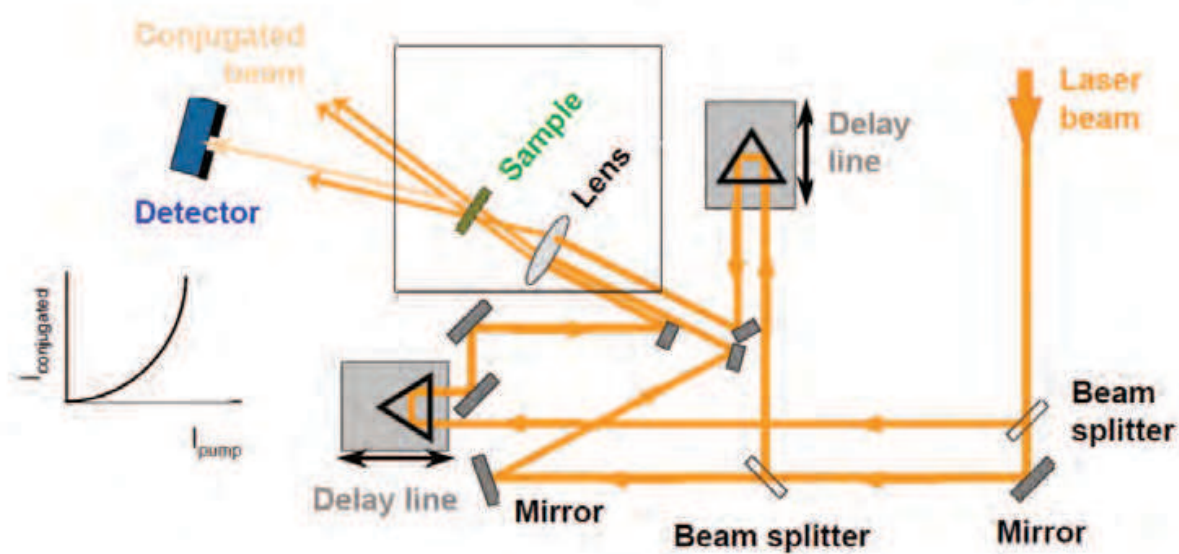
Fig. 13. Experimental DFWM setup.

fs pulses tunable in the 300–3000 nm interval. The laser pulse intensity is controlled by a $\lambda/2$ wave plate and a polarizer. Two beam splitters provide three beams with equal intensity in order to satisfy the maximum conjugate signal condition. The three beams propagate the same optical path by adjusting two delay lines. The system is aligned so that each beam lies on one vertex of a square in order to guarantee the wave vector conservation rule and at 4 mm of the center of the lens for minimizing lens aberrations. The conjugate signal is detected far away from the position of the sample, where the spatially filtered pumps and probe beams are enough separated to improve the signal-to-noise ratio. More details about the experimental setup can be found in Ref. (del Coso López, 2004).

In order to obtain the dependence of the intensity of the conjugate signal with the third-order susceptibility it is necessary to solve the nonlinear wave equation, where the nonlinear polarization $\mathbf{P}_{NL}^{(3)}(\omega)$ acts as an electric field **source term** at the given frequency. Assuming the monochromatic components of the electric field $\mathbf{E}(\omega)$ polarized in the $x$ and $y$ direction and propagating along the $z$ direction, the electric field associated to the conjugate beam can be written (Shutherland, 2003) as:

$$\frac{\partial E_c(\omega)}{\partial z} = j\frac{2\omega}{\epsilon_0 n_0 c}P_c^{(3)}(\omega)e^{-jkz}$$

$$\Rightarrow \frac{\partial E_c(\omega)}{\partial z} = j\frac{3\omega}{n_0 c}\chi_{cp_1 p_2 s}^{(3)}(\omega)E_{p_1}(\omega)E_{p_2}(\omega)E_s^*(\omega)e^{-j\Delta kz} \tag{5}$$

where $\chi^{(3)}(\omega)$ denotes the three possible complex components of the third-order susceptibility tensor for generating $\omega$ and $\mathbf{k}$ is the wave vector, or change in phase per length unity along the path traveled by the wave. The last term of the previous equation leads to an exponential attenuation of the conjugate signal unless the term

$$\Delta \mathbf{k} = \mathbf{k}_{p_1} + \mathbf{k}_{p_2} - \mathbf{k}_s - \mathbf{k}_c \tag{6}$$

is equal to zero. This implies that for maximizing the conjugated signal, the phase matching condition $\sum \mathbf{k_i}$=0 has to be fulfilled. This is straightforward in the boxcar configuration.

Taking into account the boundary conditions given by the input beams, the solution of the nonlinear wave equation can be obtained for low conversion efficiency ($I_c << I_{p_1}, I_{p_2}, I_s$) and absorbing media ($\alpha_0 \neq 0$). The intensity of the conjugate signal is then given by:

$$I_c \cong \left( \frac{3\pi L_{eff}}{\epsilon_0 n_0^2 c\lambda} \right)^2 e^{-\alpha L} \left| \chi_{cp_1p_2s}^{(3)} \right| I_{p_1} I_{p_2} I_s \tag{7}$$

From this equation we can obtain the third-order nonlinear susceptibility $\left| \chi_{cp_1p_2s}^{(3)} \right|$ by measuring the intensity of the conjugate beam as a function of the intensity of the pumps and probe beams. The maximum conjugate beam intensity is obtained for equally intense pump and probe beams from Eq. 7, hence: $I_c$ máx. $\leftrightarrow I_{p_1} = I_{p_2} = I_s = I_0/3$. Thus, the dependence of the conjugate beam intensity on the pump beam intensity follows a cubic relationship $I_c = cI_0^3$.

It is also possible to quantify the $\left| \chi_{cp_1p_2s}^{(3)} \right|$ by using a transparent (non absorbing) reference material with a known $\chi^{(3)}$ (Shutherland, 2003). Then, the third-order susceptibility of the sample under study is expressed as:

$$\left| \chi_s^{(3)} \right| = \left( \frac{n_0^s}{n_0^r} \right)^2 \left( \frac{L^r}{L^s} \right) \left( \frac{c^s}{c^r} \right)^{1/2} \frac{\alpha_0 L^s e^{-\alpha_0 L^s/2}}{1 - e^{-\alpha_0 L^s}} \left| \chi_r^{(3)} \right| \tag{8}$$

where the subscripts $r$ and $s$ stands for the reference and the sample, respectively, and $\alpha_0 L$ is the linear absorption of the sample. In this experiment, the reference used is a fused silica (SiO$_2$) plate with a well known $|\chi^{(3)}|$ = 1.28×10$^{-14}$ esu (1.79×10$^{-22}$ m$^2$/V$^2$) and $n_0$ = 1.45 (Shutherland, 2003). Throughout this chapter the cgs system of units (esu) for the quantification of $\chi^{(3)}$ is used. The conversion to SI units is given by $\chi^{(3)} \left( m^2/V^2 \right) = \frac{4\pi}{9} 10^{-8} \chi^{(3)} (esu)$.

## 5.2 QD nonlinear optical properties

### 5.2.1 Third-order susceptibility $\chi^{(3)}$

In DFWM measurements, the conjugate beam intensity $I_c$ is plotted versus the pump intensity $I_p$ to obtain the coefficient $c$ of the relationship $I_c = cI_0^3$. The third-order susceptibility $|\chi^{(3)}|$ is calculated using Eq. 8. The refractive index of the active region (GaN) considered for the estimation of the third-order susceptibility is $n_0$ = 2.2.

The third-order susceptibility of the AlN-template substrate ($\sim$1.8×10$^{-8}$ esu) was measured at 1.55 $\mu$m in order to evaluate its potential contribution to the nonlinear signal. It should be pointed out that the laser source used in the experiment is not resonant with the bandgap of the AlN ($\sim$200 nm). Thus, the nonlinear contribution of the AlN to the incident electromagnetic field should be negligible compared to the contribution of light polarized in the $z$ direction, which is absorbed by the active region of the GaN/AlN heterostructure. To avoid the nonlinear contribution of the substrate, the input power density was fixed so that the signal from the substrate remains below the experimental resolution of the setup. Thus,

it is ensured that the nonlinear response measured by DFWM is only generated by the GaN QWs or QDs and not by the substrate.
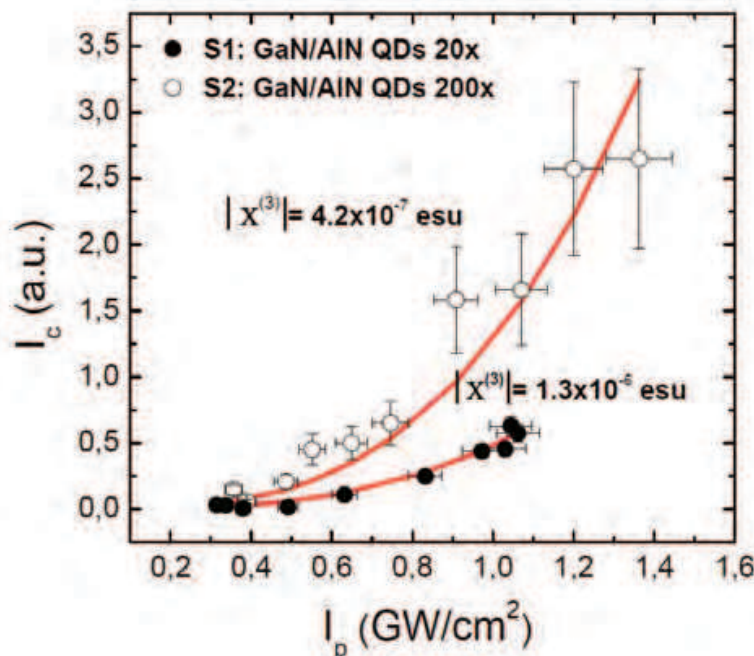


Fig. 14. $I_c$ vs. $I_p$ plot of GaN/AlN QDs samples at 1.55 $\mu$m. Solid lines correspond to the cubic data fit given by $I_c=cI_p^3$.

Figure 14 shows a representative plot of the measured conjugate-beam intensity ($I_c$) vs. the pump-beam intensity ($I_p$) for GaN/AlN QD heterostructures at 1.55 $\mu$m. The conjugate signal follows a cubic dependence on the pump power as expected from a third-order nonlinear process. The solid lines correspond to the cubic data fitted to a $I_c = cI_0^3$ curve. For sample S2, a higher value of $I_c$ is obtained due to its higher effective length since $I_c \propto L_{eff}^2$ (see Eq. 7).

Third-order susceptibility $|\chi^{(3)}|$ values of $(1.3\pm0.1)\times10^{-6}$ and $(4.2\pm0.4)\times10^{-7}$ esu were estimated at 1.55 $\mu$m for GaN/AlN QD samples S1 and S2, respectively. The obtained values increase with the linear absorption of the samples, being higher for the sample with highest Si concentration (S1) due to the increase of the intraband absorption efficiency with Si-doping. For the GaN/AlN QW sample (S3) a value of third-order susceptibility $|\chi^{(3)}|$ of $(2.4\pm0.2)\times10^{-7}$ esu was estimated at 1.55 $\mu$m (Valdueza-Felip et al., 2008).

The obtained value of $|\chi^{(3)}|$ for the GaN/AlN QW sample is very similar to the one estimated by Suzuki *et al.* of $1.6\times10^{-7}$ esu in GaN/AlN QWs at 1.55 $\mu$m (Suzuki & Iizuka, 1997). However, it is one order of magnitude larger than the experimental value achieved by Hamazaki *et al.* in GaN/AlN multiple QWs at the same wavelength (Hamazaki et al., 2004). This improvement of $|\chi^{(3)}|$ might be related to the structural properties of the samples since the absorption saturation is known to be very sensitive to the structure of the material (Iizuka et al., 2006). It must also be pointed out the use of different measurement technique (we measure the modulus of the third-order susceptibility, while Hamazaki *et al.* make an estimation of its imaginary part). The values of $|\chi^{(3)}|$ obtained in the QD samples (S1-S2) are $\approx$ 5 times larger than the one obtained in the QW sample (S3), as expected from the higher

confinement in the QDs. It is also noteworthy that GaN/AlN-based heterostructures present an increase of 4 orders of magnitude of $\chi^{(3)}$ compared to InGaAsP-InP (Donnelly et al., 1996) and InN (Naranjo et al., 2007) material systems.

### 5.2.2 Population grating lifetime $\tau$

DFWM technique allows determining the lifetime, $\tau$, of the generated population grating by adjusting the time delay between the pump and probe beams (Adachi et al., 2000). In particular, this measurement is performed by modifying the optical path length of the probe beam using an optical delay line. The pump beams interfere and generate a spatially periodic grating that interferes with the delayed probe beam. The transient response is obtained from the evolution of the intensity of the conjugate beam as a function of the probe time delay.
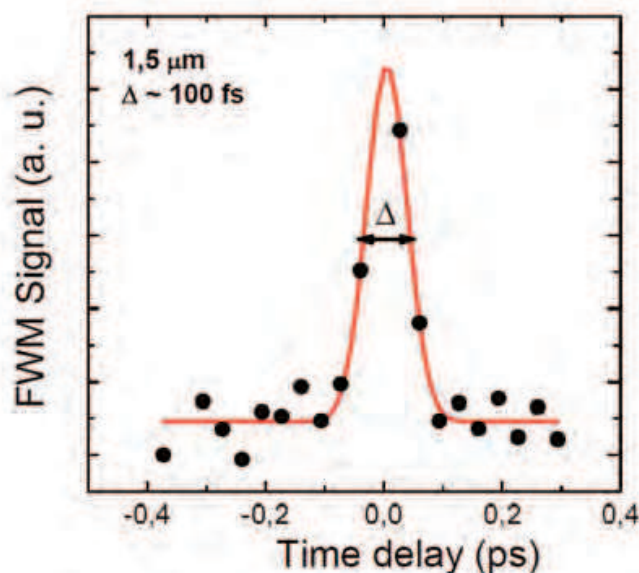


Fig. 15. DFWM signal intensity as a function of delay time between one of the pumps and the others for the GaN/AlN QD sample (S1).

Figure 15 shows the dependence of the conjugate signal intensity as a function of the time delay, obtained for the sample S1. The signal starts at zero and it increases when pump and probe beams become synchronized. It reaches its maximum when there is a full overlap in space and time of the two pump beams and the probe one in the sample. As the delay line moves away from the maximum overlap, the generated signal decays at the rhythm of the decay of the excited population in the sample. However, for the three samples under study, the measured lifetime of the population grating is smaller or comparable to the laser pulse width of 100 fs. This result is consistent with the subpicosecond intraband decay times measured in GaN QW structures, being related to a carrier relaxation process governed by the Fröhlich interaction between electrons and longitudinal-optical (LO) phonons (Hamazaki et al., 2004; Heber et al., 2002; Iizuka et al., 2006; 2000; Rapaport et al., 2003). Finally, Fig. 16 shows the figure of merit (FOM) for nonlinear optical materials: $\chi^{(3)}/\alpha$ vs. switching rate $1/\tau$, for different material systems (Hanamura et al., 2007), confirming the potential of GaN/AlN heterostructures for ultrafast all-optical devices.
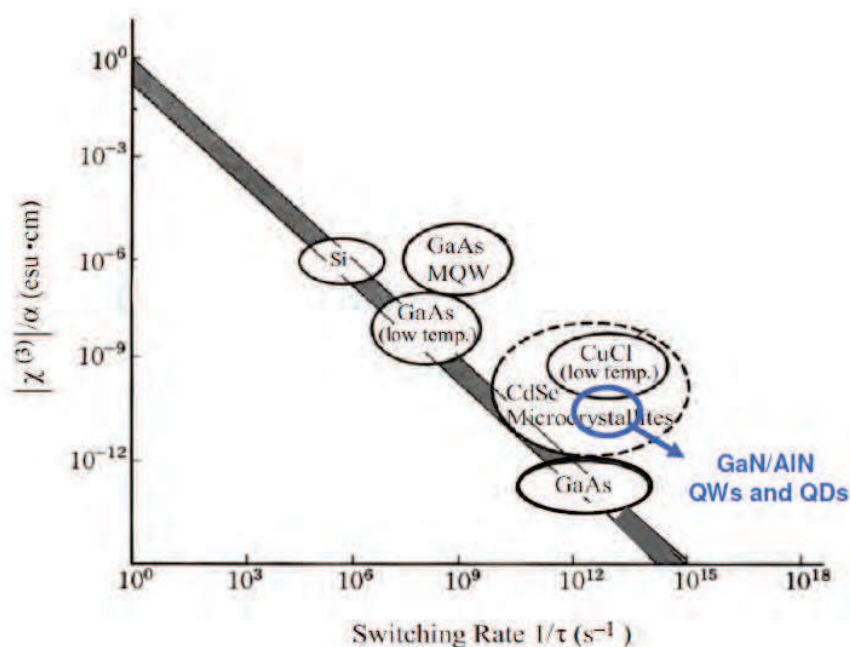
Fig. 16. Figure of merit for nonlinear optical materials: $\chi^{(3)}/\alpha$ vs. the switching rate $1/\tau$. The empirical law of constant FOM $\chi^{(3)}/\alpha$ = const. is represented by the shaded straight line (Hanamura et al., 2007).

## 6. Conclusions

In this chapter, the nonlinear properties of Si-doped GaN/AlN QD and QW superlattices have been evaluated at telecom wavelengths (1.55 $\mu$m). The samples under study present a near-infrared intraband absorption at $\sim$1.55 $\mu$m wavelength assigned to the $e_1$-$e_2$ transition in the QWs and to the $s$-$p_z$ transition in the QDs.

The nonlinear optical characterization of the samples was performed using the degenerate FWM technique in boxcars configuration. The conjugate signal intensity obtained for all the samples followed a cubic law with the pump power, as expected from a third-order nonlinear process. The measured conjugate-beam intensity is higher for the sample with the highest effective length and minimum linear absorption. On the other hand, the third-order susceptibility increases with the intraband absorption of the layer, achieving a maximum value of $|\chi^{(3)}|$ = (1.3$\pm$0.1)$\times 10^{-6}$ esu for the GaN/AlN QD sample. This value is $\approx$ 5 times larger than the one obtained in the QW sample of $|\chi^{(3)}|$ = (2.4$\pm$0.2)$\times 10^{-7}$ esu, which is consistent with results reported in the literature. This increase of $\chi^{(3)}$ for the QD sample is attributed to its higher (3D) quantum confinement.

Finally, the population grating lifetime $\tau$ was measured during the DFWM measurements, being below 100 fs for all the analyzed samples. The ultrafast nature of intraband transitions, together with the improved nonlinear optical response, render GaN/AlN heterostructures a feasible option for all-optical switching and wavelength conversion applications at 1.55 $\mu$m. The development of waveguides based on GaN/AlN heterostructures could enable new all-optical devices with potentially high speed operation, high contrast ratio and low saturation intensity suitable for future in multi-Tbit optical communication networks.

## 7. References

Adachi, S., Takagi, Y., Takeda, J. & Nelson, K. A. (2000). Optical sampling four-wave-mixing experiment for exciton relaxation processes, *Optics Communications* 174(1): 291.

Adelmann, C., Brault, J., Mula, G., Daudin, B., Lymperakis, L. & Neugebaue, J. (2003). Gallium adsorption on (0001) gan surfaces, *Phys. Rev. B* 67: 165419.

Adelmann, C., Simon, J., Feuillet, G., Pelekanos, N. T., Daudin, B. & Fishman, G. (2000). Self-assembled ingan quantum dots grown by molecular beam epitaxy, *Appl. Phys. Lett.* 76: 1570.

Akimoto, R., Simoyama, T., Tsuchida, H., Namiki, S., Lim, C. G., Nagase, M., Mozume, T., Hasama, T. & Ishikawa, H. (2007). All-optical demultiplexing of 160–10 gbit/s signals with mach-zehnder interferometric switch utilizing intersubband transition in ingaas/alas/alassb quantum well, *Appl. Phys. Lett.* 91(22): 221115.

Almeida, V. R., Barrios, C. A., Panepucci, R. R. & Lipson, M. (2004). All-optical control of light on a silicon chip, *Nature* 431: 1081.

Andreev, A. D. (2003). *ITQW proceedings*.

Andreev, A. D. & O'Reilly, E. P. (2000). Theory of the electronic structure of gan/aln hexagonal quantum dots, *Phys. Rev. B* 62: 15851.

Andreev, A. D. & O'Reilly, E. P. (2001). Optical transitions and radiative lifetime in gan/aln self-organized quantum dots, *Appl. Phys. Lett.* 79: 521.

Bernardini, F., Fiorentini, V. & Bosin, A. (1997). Spontaneous polarization and piezoelectric constants of iii-v nitrides, *Appl. Phys. Lett.* 70: 2990.

Bloembergen, N. (2000). Nonlinear optics: past, present, and future, *IEEE J. Selected Topics in Quantum Electronics* 6(6): 876.

Boyd, R. W. (2008). *Nonlinear optics*, 3rd edn, Academic Press.

Chamard, V., Schülli, T., Sztucki, M., Metzger, T. H., Sarigiannidou, E., Rouviére, J.-L., Tolan, M., Adelmann, C. & Daudin, B. (2004). Strain distribution in nitride quantum dots multilayers, *Phys. Rev. B* 69: 125327.

Damilano, B., Grandjean, N., Dalmasso, S. & Massies, J. (1999). Room-temperature blue-green emission from ingan/gan quantum dots made by strain-induced islanding growth, *Appl. Phys. Lett.* 75: 3751.

del Coso López, R. (2004). *Propiedades ópticas no-lineales de nanocompuestos metal-dieléctrico de Cu:Al$_2$O$_3$*, PhD thesis, Universidad Autónoma de Madrid.

del Coso, R. & Solís, J. (2004). Relation between nonlinear refractive index and third-order susceptibility in absorbing media, *J. Opt. Soc. Am. B* 21(3): 640.

Donnelly, J. P., Le, H. Q., Swanson, E. A., Groves, S. H., Darwish, A. & Ippen, E. P. (1996). Nondegenerate four-wave mixing wavelength conversion in low-loss passive ingaaspŰinp quantum-well waveguides, *IEEE Photon. Technol. Lett.* 8(5): 623.

Gacevic, Z., Das, A., Teubert, J., Kotsar, Y., Kandaswamy, P. K., Kehagias, T., Koukoula, T., Komninou, P. & Monroy, E. (2011). Internal quantum efficiency of iii-nitride quantum dot superlattices grown by plasma-assisted molecular-beam epitaxy, *J. Appl. Phys.* 109(10): 103501.

Gogneau, N., Jalabert, D., Monroy, E., Shibata, T., Tanaka, M. & Daudin, B. (2003). Structure of gan quantum dots grown under "modified stranski-krastanow" conditions on aln, *J. Appl. Phys.* 94: 2254.

Gogneau, N., Jalabert, G., Monroy, E., Sarigiannidou, E., Rouviére, J.-L., Shibata, T., Tanaka, M., Gérard, J.-M. & Daudin, B. (2004). Influence of aln overgrowth on structural

properties of gan quantum wells and quantum dots grown by plasma-assisted molecular beam epitaxy, *J. Appl. Phys.* 96: 1104.

González-Herráez, M. (2011). *Advanced Fibre Optics: Concepts and Technology*, EPFL Press.

Guillot, F., Bellet-Amalric, E., Monroy, E., Tchernycheva, M., Nevou, L., Doyennette, L., Julien, F. H., Dang, L. S., Remmele, T., Albrecht, M., Shibata, T. & Tanaka, M. (2006). Si-doped gan/aln quantum dot superlattices for optoelectronics at telecommunication wavelengths, *J. Appl. Phys.* 100: 044326.

Hamazaki, J., Matsui, S., Kunugita, H., Ema, K., Kanazawa, H., Tachibana, T., Kikuchi, A. & Kishino, K. (2004). Ultrafast intersubband relaxation and nonlinear susceptibility at 1.55 $\mu$m in gan/aln multiple-quantum wells, *Appl. Phys. Lett.* 84(7): 1102.

Hanamura, E., Kawabe, Y. & Yamanaka, A. (2007). *Quantum Nonlinear Optics*, Springer-Verlag.

Heber, J. D., Gmachl, C., Ng, H. M. & Cho, A. Y. (2002). Comparative study of ultrafast intersubband electron scattering times at ∼1.55 $\mu$m wavelength in gan/algan heterostructures, *Appl. Phys. Lett.* 81(7): 1237.

Hermann, M., Monroy, E., Helman, A., Baur, B., Albrecht, M., Daudin, B., Ambacher, O., Stutzmann, M. & Eickhoff, M. (2004). Vertical transport in group iii-nitride heterostructures and application in aln/gan resonant tunneling diodes, *Phys. Stat. Sol. (c)* 1: 2210.

Hill, K., Johnson, D., Kawasaki, B. & MacDonald, R. (1978). Cw three wave mixing in single-mode optical fibers, *J. Appl. Phys.* 49: 5098.

Hofstetter, D., Baumann, E., Giorgetta, F. R., Théron, R., Wu, H., Schaff, W. J., Dawlaty, J., George, P. A., Eastman, L. F., Rana, F., Kandaswamy, P. K., Leconte, S. & Monroy, E. (2009). Photodetectors based on intersubband transitions using iii-nitride superlattice structures, *J. Phys.: Condens. Matter* 21: 174208.

Hofstetter, D., Francesco, J. D., Kandaswamy, P. K., Das, A., Valdueza-Felip, S. & Monroy, E. (2010). Performance improvement of alnŰgan-based intersubband detectors by using quantum dots, *IEEE Photon. Technol. Lett.* 22(15): 1087.

Iizuka, N., Kaneko, K. & Suzuki, N. (2006). Polarization dependent loss in iii-nitride optical waveguides for telecommunication devices, *J. Appl. Phys.* 99(9): 093107.

Iizuka, N., Kaneko, K., Suzuki, N., Asano, T., Noda, S. & Wada, O. (2000). Ultrafast intersubband relaxation (<150 fs) in algan/gan multiple quantum wells, *Appl. Phys. Lett.* 77(5): 648.

Inoue, K. (1992). Four-wave mixing in an optical fiber in the zero-dispersion wavelength region, *J. Lightwave Technology* 10: 1553.

Kandaswamy, P. K., Bougerol, C., Jalabert, D., Ruterana, P. & Monroy, E. (2009). Strain relaxation in short-period polar gan/aln superlattices, *J. Appl. Phys.* 106(1): 013526.

Kandaswamy, P. K., Guillot, F., Bellet-Amalric, E., Monroy, E., Nevou, L., Tchernycheva, M., Michon, A., Julien, F. H., Baumann, E., Giorgetta, F. R., Hofstetter, D., Remmele, T., Albrecht, M., Birner, S. & Dang, L. S. (2008). Gan/aln short-period superlattices for intersubband optoelectronics: A systematic study of their epitaxial growth, design, and performance, *J. Appl. Phys.* 104(9): 093501.

Kheirodin, N., Nevou, L., Machhadani, H., Crozat, P., Vivien, L., Tchernycheva, M., Lupu, A., Julien, F., Pozzovivo, G., Golka, S., Strasser, G., Guillot, F. & Monroy, E. (2008). Electrooptical modulator at telecommunication wavelengths based on gan-aln coupled quantum wells, *Photon. Technol. Lett.* 20(9): 724.

Li, Y., Bhattacharyya, A., Thomidis, C., Liao, Y., Moustakas, T. D. & Paiella, R. (2008). Refractive-index nonlinearities of intersubband transitions in gan/aln quantum-well waveguides, *J. Appl. Phys.* 104(8): 083101.

Moumanis, K., Helman, A., Fossard, F., Tchernycheva, M., Lusson, A., Julien, F. H., Damilano, B., Grandjean, N. & Massies, J. (2003). Intraband absorptions in gan/aln quantum dots in the wavelength range of 1.27Ű2.4 $\mu$m, *Appl. Phys. Lett.* 82: 868.

Nakamura, T., Mochizuki, S., Terao, S., Sano, T., Iwaya, M., Kamiyama, S., Amano, H. & Akasaki, I. (2002). Structural analysis of si-doped algan/gan multi-quantum wells, *J. Cryst. Growth* 1129: 237Ű–239.

Naranjo, F. B., González-Herráez, M., Fernández, H., Solís, J. & Monroy, E. (2007). Third order nonlinear susceptibility of inn at near band-gap wavelengths, *Appl. Phys. Lett.* 90(9): 091903.

Naranjo, F. B., Kandaswamy, P. K., Valdueza-Felip, S., Calvo, V., González-Herráez, M., Martín-López, S., Corredera, P., Méndez, J. A., Mutta, G. R., Lacroix, B., Ruterana, P. & Monroy, E. (2011). Nonlinear absorption of inn/ingan multiple-quantum-well structures at optical telecommunication wavelengths, *Appl. Phys. Lett.* 98(3): 031902.

Nevou, L., Julien, F. H., Tchernycheva, M., Guillot, F., Monroy, E. & Sarigiannidou, E. (2008). Intraband emission at $\lambda \approx 1.48$ $\mu$m from gan/aln quantum dots at room temperature, *Appl. Phys. Lett.* 92(16): 161105.

Nevou, L., Mangeney, J., Tchernycheva, M., Julien, F. H., Guillot, F. & Monroy, E. (2009). Ultrafast relaxation and optical saturation of intraband absorption of gan/aln quantum dots, *Appl. Phys. Lett.* 94(13): 132104.

Nevou, L., Tchernycheva, M., Julien, F. H., Raybaut, M., Godard, A., Rosencher, E., Guillot, F. & Monroy, E. (2006). Intersubband resonant enhancement of second-harmonic generation in gan/aln quantum wells, *Appl. Phys. Lett.* 89: 151101.

Radic, S. & McKinstrie, C. J. (2005). Optical amplification and signal processing in highly nonlinear optical fiber, *IEICE Trans. Electronics* E88-C(5): 859.

Ranjan, V., Allan, G., Priester, C. & Delerue, C. (2003). Self-consistent calculations of the optical properties of gan quantum dots, *Phys. Rev. B* 68: 115305.

Rapaport, R., Chen, G., Mitrofanov, O., Gmachl, C., Ng, H. M. & Chu, S. N. G. (2003). Resonant optical nonlinearities from intersubband transitions in gan/aln quantum wells, *Appl. Phys. Lett.* 83(2): 263.

Renard, J., Kandaswamy, P. K., Monroy, E. & Gayral, B. (2009). Suppression of nonradiative processes in long-lived polar gan/aln quantum dots, *Appl. Phys. Lett.* 95: 131903.

Sarigiannidou, E., Monroy, E., Daudin, B., Rouviére, J. & Andreev, A. (2005). Strain distribution in gan/aln quantum dots superlattices, *Appl. Phys. Lett.* 87: 203112.

Sarigiannidou, E., Monroy, E., Gogneau, N., Radtke, G., Bayle-Guillemaud, P., Bellet-Amalric, E., Daudin, B. & Rouviére, J. L. (2006). Comparison of the structural quality in ga-face and n-face polarity gan/aln multiple-quantum-well structures, *Semicond. Sci. Technol.* 21: 912.

Sénés, M., Smith, K. L., Smeeton, T. M., Hooper, S. E. & Heffernan, J. (2007). Strong carrier confinement in in$_x$ga$_{1-x}$n/gan quantum dots grown by molecular beam epitaxy, *Phys. Rev. B* 75: 045314.

Sheik-Bahae, M., Said, A., Wei, T., Hagan, D. & Stryland, E. V. (1990). Sensitive measurements of optical nonlinearities using a single beam, *IEEE J. Quantum Electronics* 26: 760.

Shutherland, R. L. (2003). *Handbook of Nonlinear Optics*, 2nd edn, Marcel Dekker.

Suzuki, N. & Iizuka, N. (1997). Feasibility study on ultrafast nonlinear optical properties of 1.55-$\mu$m intersubband transition in algan/gan quantum wells, *Jpn. J. Appl. Phys.* 36(Part 2, No. 8A): L1006.

Tchernycheva, M., Nevou, L., Doyennette, L., Helman, A., Colombelli, R., Julien, F. H., Guillot, F., Monroy, E., Shibata, T. & Tanaka, M. (2005). Intraband absorption of doped gan/aln quantum dots at telecommunication wavelengths, *Appl. Phys. Lett.* 87: 101912.

Tchernycheva, M., Nevou, L., Doyennette, L., Julien, F. H., Warde, E., Guillot, F., Monroy, E., Bellet-Amalric, E., Remmele, T. & Albrecht, M. (2006). Systematic experimental and theoretical investigation of intersubband absorption in gan/aln quantum wells, *Phys. Rev. B* 73(12): 125347.

Valdueza-Felip, S. (2011). *Nitride-based semiconductor nanostructures for applications in optical communications at 1.55 μm*, PhD thesis, University of Alcalá.

Valdueza-Felip, S., Naranjo, F.B., González-Herráez, M., Fernández, H., Solís, J., Guillot, F., Monroy, E., Nevou, L., Tchernycheva, M. & Julien, F. H. (2008). Characterization of the resonant third-order nonlinear susceptibility of si-doped gan/aln quantum wells and quantum dots at 1.5 *μ*m, *IEEE Photon. Technol. Lett.* 20: 1366.

Vardi, A., Kheirodin, N., Nevou, L., Machhadani, H., Vivien, L., Crozat, P., Tchernycheva, M., Colombelli, R., Julien, F. H., Guillot, F., Bougerol, C., Monroy, E., Schacham, S. & Bahir, G. (2008). High-speed operation of gan/algan quantum cascade detectors at ≈1.55 *μ*m, *Appl. Phys. Lett.* 93: 193509.

Wada, O. (2004). Femtosecond all-optical devices for ultrafast communication and signal processing, *New J. Physics* 6: 183.

Zeldovich, B. Y., Pilipetskii, N. F. & Shkunov, V. V. (1985). *Principles of Phase Conjugation*, Vol. 42 of *Springer Series in Optical Sciencies*, Springer Verlag.
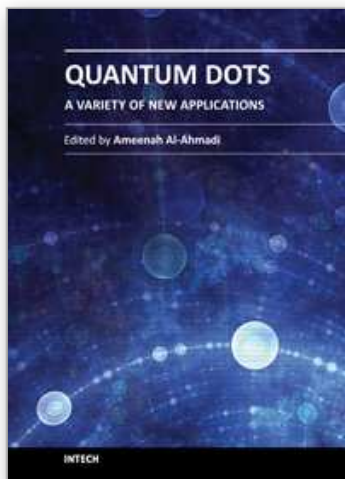
**Quantum Dots - A Variety of New Applications**

Edited by Dr. Ameenah Al-Ahmadi

The book "Quantum dots: A variety of a new applications" provides some collections of practical applications of quantum dots. This book is divided into four sections. In section 1 a review of the thermo-optical characterization of CdSe/ZnS core-shell nanocrystal solutions was performed. The Thermal Lens (TL) technique was used, and the thermal self-phase Modulation (TSPM) technique was adopted as the simplest alternative method. Section 2 includes five chapters where novel optical and lasing application are discussed. In section 3 four examples of quantum dot system for different applications in electronics are given. Section 4 provides three examples of using quantum dot system for biological applications. This is a collaborative book sharing and providing fundamental research such as the one conducted in Physics, Chemistry, Biology, Material Science, Medicine with a base text that could serve as a reference in research by presenting up-to-date research work on the field of quantum dot systems.

**How to reference**

In order to correctly reference this scholarly work, feel free to copy and paste the following:

S. Valdueza-Felip, F. B. Naranjo, M. González-Herráez, E. Monroy and J. Solís (2012). Ultrafast Nonlinear Optical Response in GaN/AlN Quantum Dots for Optical Switching Applications at 1.55 μm, Quantum Dots - A Variety of New Applications, Dr. Ameenah Al-Ahmadi (Ed.), ISBN: 978-953-51-0483-4, InTech, Available from: http://www.intechopen.com/books/quantum-dots-a-variety-of-new-applications/ultrafast-nonlinear-optical-response-in-gan-aln-quantum-dots-for-optical-switching-applications-at-1

# INTECH

open science | open minds